

# Preliminary Measurements of $B^0$ and $B^+$ Lifetimes at SLD<sup>1</sup>

The SLD Collaboration<sup>2</sup>

*Stanford Linear Accelerator Center  
Stanford University  
Stanford, CA 94309*

## ABSTRACT

The lifetimes of  $B^0$  and  $B^+$  mesons have been measured using a sample of 150,000 hadronic  $Z^0$ 's collected by the SLD experiment at the SLC between 1993 and 1995. Two analyses are presented. The first identifies semileptonic decays of  $B$  mesons with high ( $p, p_t$ ) leptons and reconstructs the  $B$  meson decay length and charge by vertexing the lepton with a partially reconstructed  $D$  meson. This method results in a sample of 428 (549) neutral (charged) decays with high charge purity. A maximum likelihood fit procedure finds:

$$\begin{aligned}\tau_{B^0} &= 1.60_{-0.14}^{+0.15}(\text{stat}) \pm 0.10(\text{syst}) \text{ ps}, \\ \tau_{B^+} &= 1.49_{-0.10}^{+0.11}(\text{stat}) \pm 0.05(\text{syst}) \text{ ps}, \\ \tau_{B^+}/\tau_{B^0} &= 0.94_{-0.12}^{+0.14}(\text{stat}) \pm 0.07(\text{syst}).\end{aligned}$$

The second analysis isolates a sample of  $B$  meson decays with a 2-D impact parameter tag and reconstructs the decay length and charge using a novel topological vertex reconstruction method. This results in a high statistics sample of 3382 (5303) neutral (charged) decays with good charge purity. A maximum likelihood fit procedure finds:

$$\begin{aligned}\tau_{B^0} &= 1.55 \pm 0.07(\text{stat}) \pm 0.12(\text{syst}) \text{ ps}, \\ \tau_{B^+} &= 1.67 \pm 0.06(\text{stat}) \pm 0.09(\text{syst}) \text{ ps}, \\ \tau_{B^+}/\tau_{B^0} &= 1.08_{-0.08}^{+0.09}(\text{stat}) \pm 0.10(\text{syst}).\end{aligned}$$

---

This work was supported by Department of Energy contacts: DE-FG02-91ER40676(BU), DE-FG03-92ER40701 (CIT), DE-FG03-91ER40618 (UCSB), DE-FG03-92ER40689 (UCSC), DE-FG03-93ER40788 (CSU), DE-FG02-91ER40672 (Colorado), DE-FG02-91ER40677 (Illinois), DE-AC03-76SF00098 (LBL), DE-FG02-92ER40715 (Massachusetts), DE-AC02-76ER03069 (MIT), DE-FG06-85ER40224 (Oregon), DE-AC03-76SF00515 (SLAC), DE-FG05-91ER40627 (Tennessee), DE-AC02-76ER00881 (Wisconsin), DE-FG02-92ER40704 (Yale); National Science Foundation grants: PHY-91-13428 (UCSC), PHY-89-21320 (Columbia), PHY-92-04239 (Cincinnati), PHY-88-17930 (Rutgers), PHY-88-19316 (Vanderbilt), PHY-92-03212 (Washington); the UK Science and Engineering Research Council (Brunel and RAL); the Istituto Nazionale di Fisica Nucleare of Italy (Bologna, Ferrara, Frascati, Pisa, Padova, Perugia); and the Japan-US Cooperative research Project on High Energy Physics (Nagoya, Tohoku).

# 1 Introduction

According to the spectator model, the decay of a heavy quark is considered to proceed independently of the other light quarks in the hadron. This model predicts that the lifetimes of all hadrons containing a given heavy quark  $Q$  are determined by the lifetime of that quark and are, therefore, equal. However, the hierarchy observed in the charm system,  $\tau_{D^+} > \tau_{D^0} \sim \tau_{D_s^+} > \tau_{\Lambda_c^+}$ , indicates the need for corrections to this model. In the  $b$ -quark system a similar hierarchy,  $\tau_{B^+} > \tau_{B^0} \sim \tau_{B_s^0} > \tau_{\Lambda_b^0}$ , is expected. Here the lifetime differences are expected to be less than 10% since they scale with  $1/m_Q^2$ . A QCD calculation using an expansion in the inverse powers of the  $b$  quark mass predicts  $\tau_{B^+}/\tau_{B^0} = 1.0 + 0.05 \times \left(\frac{f_B}{200 \text{ MeV}}\right)^2$ , where  $f_B$  is the  $B$  meson decay constant [1]. Thus, measurements of the  $B^0$  and  $B^+$  lifetimes and their ratio provide tests of deviations from the spectator model.

To determine the  $B^0$  and  $B^+$  lifetimes, the 1993 data sample of 50,000 hadronic  $Z^0$  decays (with an average beam polarization of  $(63.0 \pm 1.1)\%$ ) collected by the SLD Large Detector (SLD) at the SLAC Linear Collider (SLC) is combined with an additional 100,000 hadronic  $Z^0$  decays (with an average beam polarization of  $(77.3 \pm 0.6)\%$ ) collected in 1994 and 1995. Two analyses are presented. In the first, the semileptonic analysis, the goal is to reconstruct the total charge of tracks produced in  $B$  meson semileptonic decays. The algorithm reconstructs both  $B$  and  $D$  vertices, and takes into consideration the existence of decays of the type  $B^0 \rightarrow D^{*-}l^+\nu$  or  $B^0 \rightarrow D^{**0}l^+\nu$ , in which a slow transition pion, with charge opposite that of the lepton, is produced at the  $B$  decay vertex. This technique does not rely on the charge correlation between the lepton and the  $D$  vertex to determine the total charge of the  $B$  meson. It should be noted that a fraction of decays of the type  $B^+ \rightarrow \bar{D}^{*0}l^+\nu$  yields two slow transition pions which tends to dilute the charge assignment purity. The method has the advantage of a high charge reconstruction purity. The goal of the second analysis, the topological analysis, is to use the high resolution 3-D vertexing to reconstruct the total charge of tracks produced in hadronic, as well as semileptonic,  $B$  meson decays. An original technique is employed which uses the parameters of high quality tracks in each hemisphere to define a vertex probability function in 3-D space. This function is used to try to identify a seed vertex to which further tracks may be associated in order to reconstruct a single secondary vertex. This vertex consists mainly of tracks of  $B$  and  $D$  decay origin. The decay length is taken from the reconstructed secondary. The charge is taken from the secondary plus the charges of tracks passing looser cuts consistent with the secondary. This analysis has the advantage of almost an order of magnitude more decays than the semileptonic analysis, but with a somewhat reduced charge reconstruction purity.

The paper is organized in six main sections. The first presents a brief description of the SLD, the tracking system performance and general features common to both analyses. This is followed by a description of the semileptonic analysis, which is followed by a description of the topological analysis. A fourth section discusses the overlap of  $B$  decays between the two analyses. The fifth section discusses the contributions to the systematic error for the two measurements. The final section presents a brief summary.

## 2 The SLD

Observations of the hadronic  $Z^0$  decay products are made using the SLD [2] which consists of a Warm Iron Calorimeter (WIC) for muon identification, a Liquid Argon Calorimeter (LAC) for measuring energy flow and performing electron identification, a Cherenkov Ring Imaging Detector (CRID) for particle identification, a Central Drift Chamber (CDC) for charged track identification and momentum measurements, and a CCD pixel Vertex Detector (VXD) for precise position measurements near the interaction point. The LAC, CRID, CDC and VXD are immersed in a 0.6 T magnetic field.

The calorimetry and tracking systems are used in the analyses presented here and will be briefly discussed (reference [3] contains a detailed description). The LAC barrel covers  $|\cos\theta| < 0.84$  and endcaps cover  $0.82 < |\cos\theta| < 0.98$  for the full azimuthal range. The electromagnetic energy resolution of the calorimeter barrel is measured to be  $\sigma/E = 15\%/\sqrt{E(\text{GeV})}$ . The hadronic energy resolution is  $60\%/\sqrt{E(\text{GeV})}$ . The CDC has maximal efficiency for  $|\cos\theta| < 0.72$ . Charged tracks are reconstructed in the CDC and linked with pixel clusters in the VXD, and then a combined fit is performed. The momentum resolution of the combined fit is  $\sigma_{p_T}/p_T = \sqrt{(0.01)^2 + (0.0026/p_T)^2}$ , where  $p_T$  is the track momentum transverse to the beam direction in GeV/c.

The micron-sized SLC Interaction Point (IP) centroid position in the  $xy$  plane transverse to the beam axis is reconstructed with a measured precision of  $\sigma_{IP} = (7 \pm 2)\mu\text{m}$  using tracks in sets of  $\sim 30$  sequential hadronic  $Z^0$  decays. The  $z$  position of the  $Z^0$  primary vertex is determined on an event-by-event basis using the median  $z$  position of tracks at their point-of-closest-approach to the IP in the  $xy$  plane. The  $Z^0 \rightarrow b\bar{b}$  Monte Carlo estimates a precision of  $\sim 52\mu\text{m}$  in this quantity [3].

## 3 Semileptonic Analysis

The initial step in this analysis is to identify a track as a lepton from a  $B$  meson decay. Electron candidates are required to have energy deposits in the LAC which agree with the momentum of tracks extrapolated from the CDC, to have little or no LAC hadronic energy, and to have front/back electromagnetic energy ratio consistent with that expected for electrons[4]. Muon candidates are required to have a good match between hits found in the WIC and tracks extrapolated from the CDC, taking into account track extrapolation errors and multiple scattering[4]. To enhance the number of  $Z^0 \rightarrow b\bar{b}$  events, lepton candidates are required to pass relatively loose cuts: total momentum  $> 2$  GeV/c and momentum transverse to the nearest jet  $> 0.4$  GeV/c (where jets are found from tracks using the JADE algorithm [5] with  $y_{cut} = 0.02$ ). Application of these cuts yields a sample of 34K events.

### 3.1 *B* Vertex Reconstruction

The *B* decay vertex reconstruction proceeds separately for each event hemisphere by first reconstructing a *D* decay vertex in 3-D from a set of tracks classified as secondary. Then, the *B* decay vertex is defined by the intersection between the *D* vertex total momentum vector and the lepton direction.

The tracks used for secondary vertex reconstruction are required to have at least one associated hit in the VXD, and not to have originated from  $\gamma$  conversions, or from  $K^0$  or  $\Lambda$  decays. Furthermore, tracks are required to have either  $p > 0.8$  GeV/ $c$  or  $\delta_{3D}^{norm} \equiv \sqrt{(\delta/\sigma_\delta)^2 + (\delta_z/\sigma_{\delta_z})^2} < 3.5$  to remove residual  $\gamma$  conversion and  $K^0$  or  $\Lambda$  decay tracks ( $\delta$  is the 2-D impact parameter in the  $xy$  plane and  $\delta_z$  is the distance of closest approach along the  $z$  axis).

The remaining tracks are initially classified as secondary tracks if they satisfy  $\delta_{3D}^{norm} > 3.5$  and as primary tracks otherwise. In addition, primary tracks which form a 2-prong vertex (with any other track) which is displaced from the IP by more than  $3\sigma$  are reclassified as secondary if the vertex is  $< 1.5$  cm from the IP, but these tracks are removed from the sample if the vertex is  $> 1.5$  cm from the IP.

This track classification is used in a 3-pass algorithm to reconstruct the *B* and *D* vertices. In the first pass, the *D* vertex is formed by combining all tracks classified as secondary into a single vertex (if there is only one secondary track the second pass is attempted, see below). The *B* vertex is then formed by intersecting the *D* vertex total momentum vector with the lepton. Subsequently, an attempt is made to attach one primary track to the *B* vertex to form a 2-prong vertex.

The requirements that must be met for this assignment (or any other assignment in a later pass) to be identified as a *B* semileptonic decay are:

1. *D* vertex:
  - a. Absolute value of the charge  $\leq 1$ ,
  - b. Mass (charged tracks assumed to be  $\pi$ 's)  $< 1.9$  GeV,
  - c. Vertex displacement from IP  $> 4\sigma$ ,
  - d.  $\chi^2$  (2,3,4 prong vertex)  $< (4, 6, 7)$ .
2. *B* vertex:
  - a. Absolute value of total charge ( $B + D$ )  $\leq 1$ ,
  - b. Mass ( $B + D$  tracks)  $> 1.4$  GeV,
  - c. Observed decay length (displacement from IP)  $> 0.08$  cm,
  - d. Momentum of non-lepton track (if any)  $> 0.4$  GeV/ $c$ .

### 3. $D$ to $B$ Linking:

- a. Distance between  $D$  and  $B$  vertices  $> 200 \mu\text{m}$ ,
- b. 1-prong  $B$ : Distance of closest approach of  $D$  vector with lepton,  $< (130, 100, 70) \mu\text{m}$  for (2, 3, 4) prong  $D$  vertices,  
 2-prong  $B$ : Three-dimensional impact parameter of  $D$  vector with respect to the  $B$  vertex  $< 200 \mu\text{m}$ .

In the second pass, if there was more than one secondary track in the hemisphere, an attempt is made to add one of the remaining primary tracks to the existing  $D$  vertex. If there was only one secondary track in the hemisphere, a 2-prong vertex is formed by combining the lone secondary track with a primary track. If more than one primary track can be added to the  $D$  vertex or combined with the lone secondary track, the track which gives the smallest distance of closest approach between the lepton and the  $D$  momentum vector is chosen. If the resulting  $B$  and  $D$  vertices satisfy the above cuts the algorithm stops.

If both first and second passes fail, a final pass is attempted in which one secondary track is combined with the lepton to form the  $B$  vertex and one or more primary tracks are combined with the secondary tracks to form the  $D$  vertex.

	$B$ Vertex	$D$ Vertex
$B^0$	1 prong 2 prong	3 prong 2 or 4 prong
$B^+$	1 prong	2 or 4 prong

Table 1: Topologies reconstructed by the semileptonic analysis.

The  $B$  decay topologies reconstructed by this algorithm are listed in table 1. As observed in this table, only neutral  $D$  vertices are accepted in the selection of  $B^+$  decay candidates since  $B^+$  semileptonic decays are expected to produce mostly  $\bar{D}^0$  mesons.

## 3.2 Event Sample and Cross Checks

From the initial sample of 150K hadronic  $Z^0$  decays the analysis described above isolates 977 semileptonic  $B$  decays. Of these, 428 are reconstructed as neutral decays and 549 as charged decays. Monte Carlo studies indicate that the neutral sample is 98.7% pure in  $B$  hadrons consisting of 15.8%  $B_u^+$ , 65.4%  $B_d^0$ , 13.6%  $B_s^0$ , and 3.9%  $B$  baryons. Similarly, the charged sample is 94.9% pure in  $B$  hadrons consisting of 70.1%  $B_u^+$ , 18.4%  $B_d^0$ , 4.1%  $B_s^0$ , and 2.3%  $B$  baryons. Note that within the neutral (charged) sample there is an excess of  $B_d^0(B_u^+)$  decays over  $B_u^+(B_d^0)$  decays by about a factor of four. The rate of lepton misidentification is 8.9% (6.9%) for the neutral (charged) sample in the Monte Carlo.

Two checks of the charge assignment algorithm are performed. In the first, the requirements on the  $D$  and  $B$  charges are removed and the Monte Carlo compared with the data. The resulting charge distributions are shown in figure 1 and display good agreement between data and Monte Carlo. In particular, figure 1(a) displays the charge distribution resulting from the lepton-slow transition pion vertex (from  $D^*$  and  $D^{**}$  decays) showing excellent agreement between data and Monte Carlo. Figure 1(a) also indicates that the track combined with the lepton to form a 2-prong  $B$  vertex most often has charge opposite that of the lepton, as expected for  $D^*$  decays. The second test takes advantage of the electron beam polarization. The Forward-Backward asymmetry is formed using the thrust axis to approximate the angle ( $\cos \theta$ ) the  $b$  quark makes with the electron beam and using the sign of the lepton to determine the charge of the  $b$  quark. This asymmetry is formed separately for the left- and right-handed electron polarizations and for decays reconstructing as neutral and charged. The left and right samples are combined to form the Left-Right Forward-Backward asymmetries [4] for neutral and charged decays, as shown in figure 2. The presence of  $B^0$ - $\bar{B}^0$  mixing causes the dilution of the asymmetry observable in the neutral plot. In the limit of random charge assignment both plots would display the same asymmetry. Figure 2 also shows the good agreement between the data and Monte Carlo for the neutral and charged asymmetries.

### 3.3 Lifetime Fits

The lifetime is extracted from the decay length distribution of the selected secondary vertices using a binned maximum likelihood technique. The distributions for the neutral and charged samples, shown in figure 3, are fitted simultaneously to determine two parameters: the lifetime ratio  $\tau_{B^+}/\tau_{B^0}$  and either the  $B^0$  or the  $B^+$  lifetime. The values of the ratio are varied between 0.6 and 1.4, and the  $B^0$  or  $B^+$  lifetimes are varied between 1.0 and 2.0 ps in the fit. For each set of parameters, Monte Carlo decay length distributions are obtained by reweighting the original Monte Carlo decay length distributions for  $B^0$  and  $B^+$  with

$$W(t, \tau) = \frac{\frac{1}{\tau} e^{-t/\tau}}{\frac{1}{\tau_{gen}} e^{-t/\tau_{gen}}}, \quad (1)$$

where  $\tau$  is the desired  $B^0$  or  $B^+$  lifetime,  $\tau_{gen}$  is the lifetime value used in the Monte Carlo generation, i.e. 1.55 ps, and  $t$  is the proper time of each decay.

The maximum likelihood fit yields lifetimes of:

$$\begin{aligned} \tau_{B^0} &= 1.60_{-0.14}^{+0.15} \text{ ps}, \\ \tau_{B^+} &= 1.49_{-0.10}^{+0.11} \text{ ps}, \end{aligned}$$

with a lifetime ratio of:

$$\frac{\tau_{B^+}}{\tau_{B^0}} = 0.94_{-0.12}^{+0.14}.$$

The best fit Monte Carlo distributions (the overlays in figure 3) have a  $\chi^2 = 24.2(19.1)$  for 18 degrees of freedom for the neutral(charged) sample.

## 4 Topological Analysis

The goal of the topological analysis is to associate tracks with a single reconstructed secondary vertex in an event hemisphere in order to reconstruct the charge of the  $B$  meson decay. Such tracks result both from the  $B$  and the cascade  $D$  decays (as well as background, primarily from the IP) and hence do not originate at a true common vertex. High quality tracks are selected for use in  $B$  event tagging and vertexing. Tracks reconstructed in the CDC are required to have  $\geq 40$  hits (of a maximum of 80), have a hit at radius  $< 39$  cm, have transverse momentum  $> 400$  MeV/c, extrapolate to within 1 cm (1.5 cm) of the IP in  $xy$  ( $z$ ) and have a good fit ( $\chi^2/d.o.f. < 5$ ). In addition, after the combined CDC/VXD fit, tracks are required to have at least one associated hit in the VXD, and a combined fit  $\chi^2/d.o.f. < 5$ .

Following standard hadronic event selection cuts [3] a sample of  $Z^0 \rightarrow b\bar{b}$  enriched events is obtained. This is done by requiring that three or more tracks in an event have normalized 2-D impact parameter  $\delta/\sigma_\delta \geq 3$ . This  $Z^0 \rightarrow b\bar{b}$  event selection has an efficiency of 60% and produces a sample with a purity of 90% [3]; application of this  $b$ -tag yields 14K events.

### 4.1 Topological Vertices

The philosophy adopted by this analysis is to search for the vertices in 3-D coordinate space. To do this a function is defined (see  $V(\mathbf{r})$  below) to quantify the relative probability of the candidate vertex at  $\mathbf{r}$ . Initially, individual track probability functions,  $f_i(\mathbf{r})$ , (Gaussian tubes in 3-D space) are derived for each track  $i$ ,

$$f_i(\mathbf{r}) = \exp \left\{ -\frac{1}{2} \left[ \left( \frac{x' - (x'_0 + y'^2 \kappa)}{\sigma_1} \right)^2 + \left( \frac{z - (z_0 + \tan(\lambda)y')}{\sigma_2} \right)^2 \right] \right\}, \quad (2)$$

where the  $x, y$  coordinates have been transformed into  $x', y'$  for each track such that at  $\mathbf{r}_0$ , the point of closest approach to the IP, the track momentum is parallel to the positive  $y'$  coordinate axis in the  $xy$  plane. The first term inside the exponential includes a parabolic approximation to the circular track trajectory where  $\kappa$  is determined from the particle charge and transverse momentum, and the SLD magnetic field. The quantities  $\sigma_1$  and  $\sigma_2$  are the measurement errors for the track, at the point of closest approach, in the  $xy$  plane and  $z$  direction respectively. The trajectory is propagated into the third dimension  $z$  via the helix parameter  $\lambda$  in the second term of the exponential.

The Gaussian track function is left unnormalized so that the vertex function introduced below approximates to track multiplicity counting. The relative probability of there being a vertex at  $\mathbf{r}$  is derived taking into account that  $\geq 2$  tracks must have

$f_i(\mathbf{r}) > 0$  in this region. A smooth, continuous function is desired so that its maxima may be found. These requirements result in the form:

$$V(\mathbf{r}) = \sum_i f_i(\mathbf{r}) - \frac{\sum_i f_i^2(\mathbf{r})}{\sum_i f_i(\mathbf{r})}. \quad (3)$$

The second term on the right hand side of equation 3 insures that  $V(\mathbf{r}) = 0$  in regions where  $f_i(\mathbf{r})$  is significant for only one track. The vertex function is modified by the angular parameter  $\alpha$ ,

$$V(\mathbf{r}) \rightarrow V(\mathbf{r}) \exp(-5\alpha^2) \quad (4)$$

where the angle  $\alpha$  is defined in figure 4. The cylinder of radius  $50 \mu\text{m}$  centered on the jet axis is constructed and equation 4 is applied only on the outside in order to protect the primary vertex area. This modification biases the topological vertex finding towards the core of the jet of tracks in the hemisphere where the  $B$  decay is expected. (In the regions where the distance from the IP projected onto the jet axis is  $< -100 \mu\text{m}$  or  $> 2.5 \text{ cm}$ ,  $V(\mathbf{r})$  is set equal to zero since these locations are unlikely to contain useful vertices.) In addition, information about the size and location of the IP is folded into the definition of  $V(\mathbf{r})$ , to add extra weight to this location and to ultimately identify the tracks associated with the primary vertex.

An example of the  $xy$  projections of  $\sum_i f_i(\mathbf{r})$  and  $V(\mathbf{r})$  is shown in figure 5(a) and 5(b) respectively. These plots are obtained by integrating the function over the third dimension  $z$  within the limits of  $\pm 8 \text{ mm}$  from the IP in the  $z$  direction. The hemisphere of tracks chosen for this plot is taken from a Monte Carlo  $Z \rightarrow b\bar{b}$  event in which the jet momentum is directed from left to right in figure 5. While the trajectories of individual tracks can be seen in figure 5(a), the regions where vertices are probable can be seen from the distribution of  $V(\mathbf{r})$  in figure 5(b). In this case the algorithm resolved the hemisphere into two vertices, i.e. the primary vertex and a secondary vertex. The peak in  $V(\mathbf{r})$  produced by the primary vertex can be seen in figure 5(b) at  $x = y = 0$ , the secondary peak is displaced to the right of the IP by  $\sim 1.5 \text{ mm}$ .

The 3-D space is divided into ‘resolved’ regions which are associated with tracks to form candidate vertices. The two locations  $\mathbf{r}_1$  and  $\mathbf{r}_2$  are said to be resolved if:

$$\frac{\min\{V(\mathbf{r}) : \mathbf{r} \in \mathbf{r}_1 + \beta(\mathbf{r}_2 - \mathbf{r}_1), 0 \leq \beta \leq 1\}}{\min\{V(\mathbf{r}_1), V(\mathbf{r}_2)\}} < 0.6 \quad (5)$$

where  $\min\{V(\mathbf{r}_1), V(\mathbf{r}_2)\}$  is the lower of the two values and the numerator in equation 5 is the minimum of  $V(\mathbf{r})$  on a straight line joining  $\mathbf{r}_1$  and  $\mathbf{r}_2$ .

A 3-D spatial point is associated with all track pairs which is the nearest local maximum in  $V(\mathbf{r})$  to the point of normalized closest approach to both tracks. These spatial points are clustered into separate spatial regions using equation 5. The tracks



associated with each spatial region form a candidate vertex. If a track has a  $\chi^2$  contribution to the vertex of greater than 10 it is removed and the remaining tracks are refit. This process is repeated until no vertices contain tracks failing this  $\chi^2$  cut. Remaining ambiguities, in which a track is associated with more than one region, are decided by fixing such tracks in the region with the greatest value of  $V(\mathbf{r})$ . The final set of tracks associated with each spatial region are fit together to form the topological vertex structure.

The efficiency for reconstructing a secondary vertex is a function of the true decay length of the parent particle. The inclusive efficiency for reconstructing a secondary vertex in a  $B$  hemisphere after event selection is about 67%. The  $B$  vertex reconstruction efficiency reaches a constant maximum of over 80% for  $B$  decays more than 3 mm from the IP.

## 4.2 Charge Reconstruction

The charge is reconstructed by associating tracks with a single secondary vertex in the hemisphere. The seed of this secondary vertex is taken to be the non-primary topological vertex furthest from the IP (the fraction of hemispheres reconstructing more than one secondary vertex is 10% of the total which reconstruct at least one). A vertex axis is formed by a straight line joining the IP to this secondary, or seed, vertex (figure 6).

The transverse impact parameter  $T$  is the shortest 3-D distance between a track and the vertex axis. The distance  $L$  along the vertex axis to the point from which  $T$  is measured is also calculated for each track. Tracks which are not directly associated with the secondary vertex but which have small values of  $T$  are likely to be associated with the decay sequence. The value of  $L$  for such tracks, compared with the vertex decay length  $D$  locates the track position along the decay chain. Good quality tracks with  $T < 0.1$  cm and  $L/D > 0.3$  are added to the set of tracks forming the secondary vertex. In addition, the charge of tracks which fail the good quality selection but have transverse momentum (relative to the beam)  $> 250$  MeV/c and  $\sqrt{(\sigma_1^2 + \sigma_2^2)} < 700$   $\mu\text{m}$ , as well as  $T < 0.1$  cm and  $L/D > 0.3$ , is also added to the secondary vertex charge. All other secondary vertex properties, such as mass and decay length (the distance from the IP to the vertex formed by all high quality tracks in the secondary), are derived from the high quality tracks alone.

The neutral sample consists of hemispheres with secondary vertex charge equal to 0, while the charged sample consists of hemispheres with secondary vertex charge equal to  $\pm 1, 2$  or 3. Figure 7 shows the reconstructed charge distribution (after application of the cuts on mass and decay length to be discussed in the next section).

### 4.3 Event Sample and Cross Checks

The above procedure yields 20022 hemispheres with a reconstructed secondary vertex. A comparison of the reconstructed mass (assuming  $\pi$  tracks) of the vertex between data and Monte Carlo is shown in figure 8, which also demonstrates that essentially all of the charm contamination in the sample can be eliminated by requiring the reconstructed vertex mass be  $\geq 2$  GeV. A final cut requires that the reconstructed decay length is  $> 1$  mm. The  $B$  charge reconstruction for hemispheres failing this cut is poor due to the proximity of the IP. Application of these cuts yields a sample of 8685 reconstructed vertices with 3382 reconstructing as neutral decays and 5303 reconstructing as charged decays. Monte Carlo studies indicate that the resulting neutral sample is 99.3% pure in  $B$  hadrons consisting of 22.2%  $B_u^+$ , 55.5%  $B_d^0$ , 15.3%  $B_s^0$ , and 6.3%  $B$  baryons. Similarly, the charged sample is 99.0% pure in  $B$  hadrons consisting of 56.2%  $B_u^+$ , 29.8%  $B_d^0$ , 8.2%  $B_s^0$ , and 4.8%  $B$  baryons. Hence within the neutral (charged) sample there is an excess of  $B_d^0(B_u^+)$  decays over  $B_u^+(B_d^0)$  decays by about a factor of two.

As with the semileptonic analysis, two checks of the charge assignment can be performed. The first compares the reconstructed charge between data and Monte Carlo and is shown in figure 7. The second again uses the electron beam polarization, this time exploiting that left-handed electrons preferentially produce  $b$  quarks in the electron direction (and  $\bar{b}$  quarks in the positron direction). The distributions of the cosine of the angle between the event thrust axis and the incident positron direction ( $\cos \theta$ ), signed by the product of the electron polarization and the reconstructed vertex charge (for charged decays), are shown in figure 9 (separately for 1993 where the average electron beam polarization was 63% and 1994/95 where it was 78%).  $B^0$  decays with the wrong charge assignment will cause a dilution of the observed asymmetry tending to flatten the distributions as a function of  $\cos \theta$ . Figure 9 also illustrates the good agreement between data and Monte Carlo.

### 4.4 Lifetime Fits

The resulting decay lengths for the neutral and charged samples are shown in figure 10. A fitting procedure identical to that employed for the semileptonic analysis is used to obtain values of:

$$\tau_{B^0} = 1.55 \pm 0.07 \text{ ps,}$$

$$\tau_{B^+} = 1.67 \pm 0.06 \text{ ps,}$$

with a ratio of:

$$\frac{\tau_{B^+}}{\tau_{B^0}} = 1.08^{+0.09}_{-0.08}.$$

The best fit Monte Carlo distributions (the overlays in figure 10) have a  $\chi^2 = 37.8(48.1)$  for 38 degrees of freedom for the neutral(charged) sample.

Semileptonic	Topological	Data Number	Data Fraction	Monte Carlo Fraction
Charged	Charged	194	44%	44%
Neutral	Neutral	160	36%	39%
Charged	Neutral	27	6%	5%
Neutral	Charged	59	13%	11%
	Opposite Charge	4	1%	1%
Total:		444		

Table 2: Number of decays common to the semileptonic and topological analyses by vertex type.

## 5 Overlap Sample

The overlap of  $B$  decays between the two analyses has been studied and the numbers are presented in table 2. It is found that  $(80 \pm 2)\%$  of the decays have the same charge assignment, in good agreement with the prediction of 83% from the Monte Carlo. Figure 11 shows, for decays with the same charge assignment, the distributions of the differences between the decay lengths and the differences between the momenta of vertices reconstructed by the two analyses. The decay length difference distribution displays a shift towards negative values due to the different strategies employed to reconstruct the  $B$  meson decay length. As discussed in section 3, the semileptonic analysis attempts to explicitly reconstruct both the  $B$  and  $D$  meson vertices. In contrast, the topological analysis attempts to reconstruct the decay length using tracks from both decays, resulting in a larger decay length than found by the semileptonic analysis. An identical set of tracks is assigned to the secondary vertex in 85% of the decays with the same reconstructed charge in both analyses. This demonstrates the high level of agreement between the two analyses.

## 6 Systematic Error

Systematic uncertainties due to detector and physics modeling, as well as those related to the fitting procedure, have been investigated. Since many of these uncertainties are common to both the semileptonic and topological analyses they are treated together in this section. The individual contributions to the total systematic error estimates on the lifetimes and lifetime ratios for both analyses are summarized in table 3.

The main contribution to the systematic error due to detector modeling originates from the uncertainty in the track reconstruction efficiency. For the semileptonic analysis, the uncertainty in the rate of fake lepton identification was investigated by varying this rate by  $\pm 50\%$  in the Monte Carlo.

Systematic Error	Semileptonic			Topological		
	$\Delta\tau_{B^0}$ (ps)	$\Delta\tau_{B^+}$ (ps)	$\Delta\left(\frac{\tau^+}{\tau^0}\right)$	$\Delta\tau_{B^0}$ (ps)	$\Delta\tau_{B^+}$ (ps)	$\Delta\left(\frac{\tau^+}{\tau^0}\right)$
Detector Modeling						
Charge assignmt.	0.004	0.016	0.014	0.040	0.040	0.040
Lepton ID	0.001	0.006	0.002	–	–	–
Physics Modeling						
$b$ fragmentation	0.056	0.026	0.022	0.032	0.032	<.005
$B$ decay charm	0.009	0.006	0.007	<.005	0.020	0.020
$\text{BR}(B \rightarrow D^{**}l\nu X)$	0.011	0.004	0.006	–	–	–
$B$ decay multipl.	0.011	0.015	0.016	0.010	0.030	0.030
$B_s$ fraction	0.006	0.004	0.005	0.005	0.019	0.010
$B$ baryon fraction	0.014	0.004	0.007	0.021	0.014	0.006
$B_s$ lifetime	0.029	0.001	0.017	0.053	0.013	0.051
$B$ baryon lifetime	0.005	0.002	0.003	0.016	0.004	0.012
$B \rightarrow D$ spectrum	–	–	–	0.025	0.006	0.019
Charm hadron $\tau$	0.011	0.001	0.007	–	–	–
Monte Carlo and Fitting						
Fit systematics	0.060	0.010	0.040	0.087	0.057	0.056
MC statistics	0.042	0.030	0.039	0.021	0.018	0.027
<b>TOTAL</b>	<b>0.100</b>	<b>0.047</b>	<b>0.068</b>	<b>0.122</b>	<b>0.091</b>	<b>0.100</b>

Table 3: Summary of contributions to the systematic error for the  $B^0$  and  $B^+$  lifetime analyses

The contributions to the systematic error due to physics modeling include the uncertainties in the  $b$  quark fragmentation and the  $B$  meson decay model, as well as the sensitivity to assumptions concerning  $B_s$  and  $B$  baryon production and lifetimes. The uncertainty in  $b$  quark fragmentation was determined by varying the  $\epsilon_b$  parameter in the Peterson fragmentation function [6], corresponding to  $\langle x_E \rangle = 0.700 \pm 0.011$  [7]. The systematic error also includes a variation in the shape of the  $x_E$  distribution [8]. The branching ratios for  $B^+ \rightarrow \bar{D}^0 X$ ,  $B^+ \rightarrow D^- X$ ,  $B^0 \rightarrow \bar{D}^0 X$ , and  $B^0 \rightarrow D^- X$  were varied by the uncertainty in the current world average [9]. The average  $B^0$  and  $B^+$  decay multiplicities were varied by 0.3 tracks [10] in an anticorrelated manner. For the semileptonic analysis, we investigated the sensitivity to  $B^+ \rightarrow D^{**}l\nu$  decays which produce two “slow” charged pions at the  $B$  decay vertex in about 8% of all semileptonic decays. This rate was varied by  $\pm 100\%$  by increasing or decreasing the charged and neutral sample purities accordingly. The lifetime fit assumes particular values for the  $B_s$  and  $B$  baryon lifetimes and production fractions. These were varied according to  $\tau(B_s) = 1.55 \pm 0.15$  ps,  $\tau(B \text{ baryon}) = 1.10 \pm 0.11$  ps,  $f(B_s) = 0.12 \pm 0.04$ , and  $f(B \text{ baryon}) = 0.08 \pm 0.04$ . For the topological analysis, the  $D$  meson spectrum from  $B$  decays is not known as accurately as in the case of semileptonic decays. To account for that, an error was assigned by requiring the Monte Carlo spectra to match recent

CLEO data [11]. Finally, the lifetime of charm hadrons ( $D^+$ ,  $D^0$ ,  $D_s$ ,  $\Lambda_c$ ) was varied according to the uncertainty in their world average [9].

The largest contribution to the systematic error arises from uncertainties in the fitting procedure, and also from Monte Carlo statistics in the semileptonic analysis. The fitting uncertainties were conservatively estimated by varying the bin size used in the decay length fit distributions, and by modifying the cuts on the minimum and/or maximum decay lengths used in the fit. These effects are partly accountable for by statistics but are included until further studies are completed.

## 7 Summary

The  $B^0$  and  $B^+$  lifetimes have been measured from a sample of 150K hadronic  $Z^0$  decays collected by SLD between 1993 and 1995. The semileptonic analysis isolates 977  $B$  hadron candidates, 428 neutral and 549 charged, and determines the following preliminary values for the lifetimes of the  $B^0$  and  $B^+$  mesons:

$$\tau_{B^0} = 1.60_{-0.14}^{+0.15}(\text{stat}) \pm 0.10(\text{syst}) \text{ ps},$$

$$\tau_{B^+} = 1.49_{-0.10}^{+0.11}(\text{stat}) \pm 0.05(\text{syst}) \text{ ps},$$

with a ratio of:

$$\frac{\tau_{B^+}}{\tau_{B^0}} = 0.94_{-0.12}^{+0.14}(\text{stat}) \pm 0.07(\text{syst}).$$

The topological analysis isolates 8685  $B$  hadron candidates, 3382 neutral and 5303 charged, and determines the following preliminary values for the lifetimes of the  $B^0$  and  $B^+$  mesons:

$$\tau_{B^0} = 1.55 \pm 0.07(\text{stat}) \pm 0.12(\text{syst}) \text{ ps},$$

$$\tau_{B^+} = 1.67 \pm 0.06(\text{stat}) \pm 0.09(\text{syst}) \text{ ps},$$

with a ratio of:

$$\frac{\tau_{B^+}}{\tau_{B^0}} = 1.08_{-0.08}^{+0.09}(\text{stat}) \pm 0.10(\text{syst}).$$

The systematic errors in the two analyses are currently dominated by uncertainties in the binned maximum likelihood fit procedure and are expected to decrease with additional data. The overlap between the two analyses is found to be 444 decays (or  $\sim 45\%$  of the semileptonic sample). The results presented here are in good agreement with the current world averages.

## References

- [1] *Non-leptonic Decays of Beauty Hadrons - from Phenomenology to Theory*, I.I. Bigi *et al.*, in *B Decays*, ed. S. Stone, World Scientific (1994);  
*Lifetimes of Heavy Flavor Hadrons: Whence and Whither?* I.I. Bigi, UND-HEP-95-BIG-06 (1995).
- [2] *SLD Design Report*, G. Agnew *et al.*, SLAC-0273 (1984).
- [3] *Measurements of  $R_b$  using Impact Parameters and Displaced Vertices*, K. Abe *et al.*, SLAC-PUB-95-6569 (1995).
- [4] K. Abe *et al.*, Phys. Rev. Lett. **74**, 2895 (1995).
- [5] S. Bethke *et al.*, Phys. Lett. **213B**, 235 (1988).
- [6] C. Peterson *et al.*, Phys. Rev. **D27**, 105 (1983).
- [7] see for example,  
R. Akers *et al.*, Z. Phys. **C60**, 199 (1993);  
D. Buskulic *et al.*, Z. Phys. **C62**, 179 (1994);  
P. Abreu *et al.*, Z. Phys. **C66**, 323 (1995).
- [8] M. G. Bowler, Z. Phys. **C11**, 169 (1981).
- [9] Particle Data Group, Phys. Rev. **D50**, Part I (1994).
- [10] H. Albrecht *et al.*, Z. Phys. **C54**, 13 (1992);  
R. Giles *et al.*, Phys. Rev. **D30**, 2279 (1984).
- [11] M. Thulasidas, Ph. D. Thesis, Syracuse University (1993).

SLD Preliminary

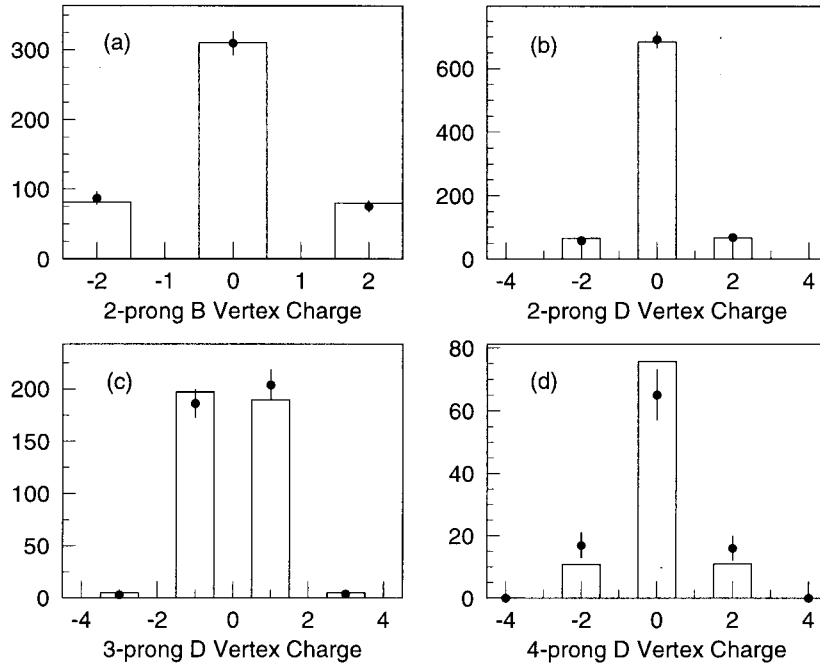


Figure 1: Comparison of charge assignment between the data (points) and Monte Carlo (histograms) for the semileptonic analysis.

SLD Preliminary

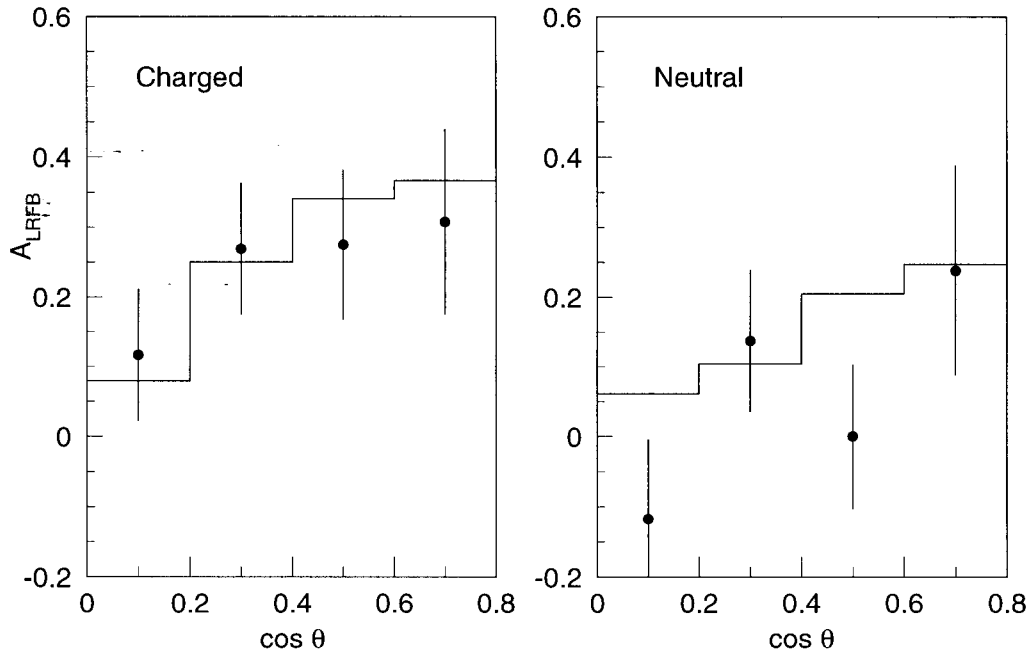


Figure 2: The Left-Right Forward-Backward asymmetry for charged and neutral decays in the semileptonic analysis for data (points) and Monte Carlo (histograms).

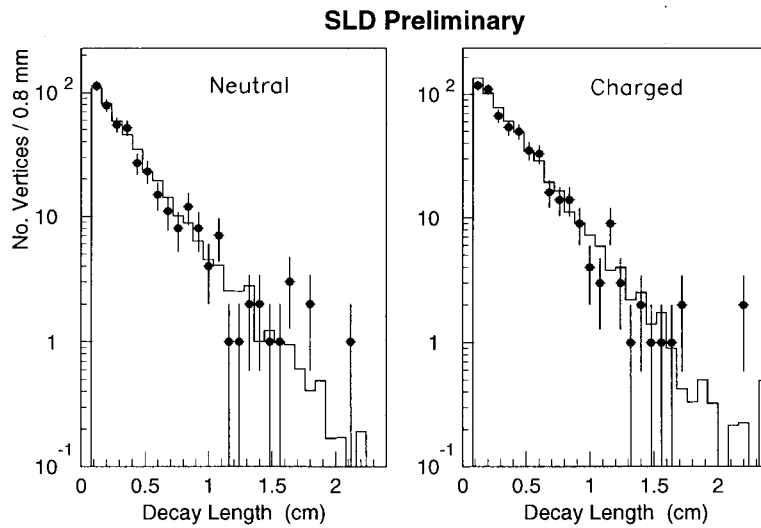


Figure 3: Decay length distributions for charged and neutral decays in the semileptonic analysis for data (points) and Monte Carlo corresponding to the best fit (histograms).

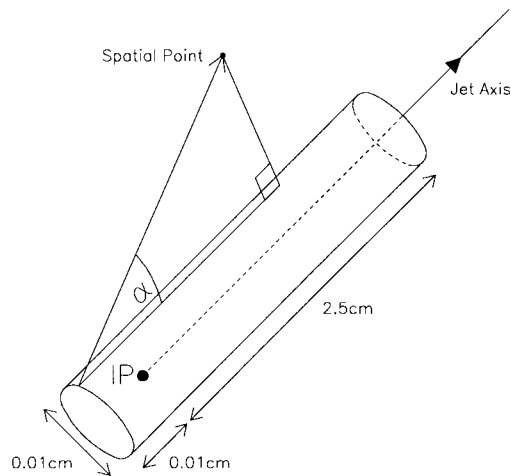


Figure 4: Construction of  $\alpha$ , the angular displacement.



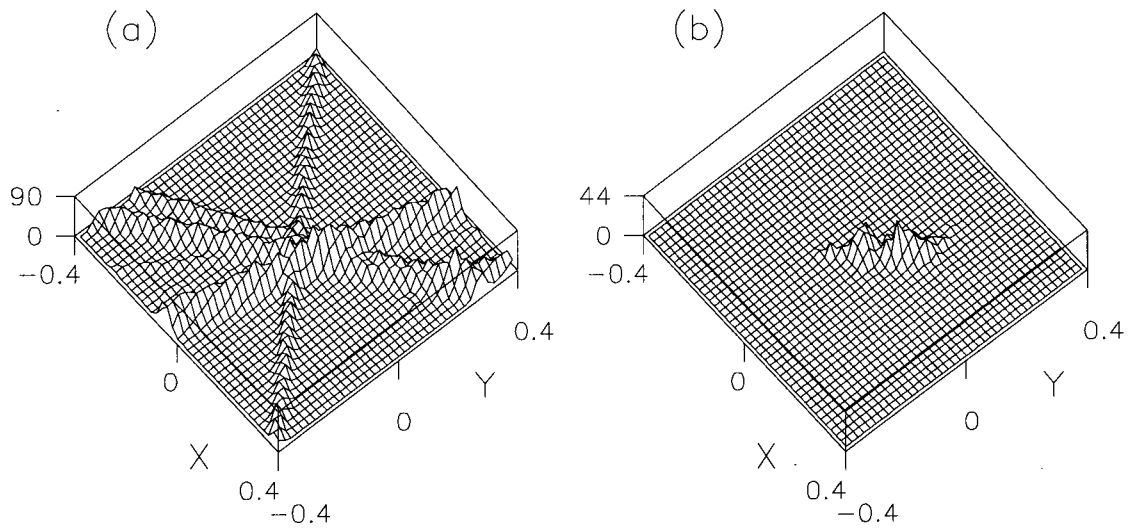


Figure 5: The track and vertex functions projected onto the  $xy$  plane.

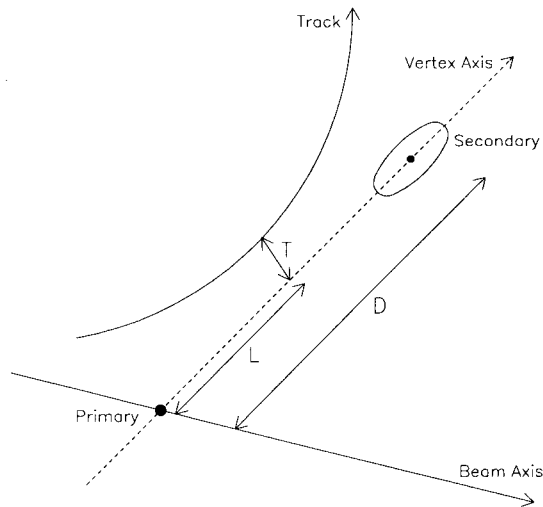


Figure 6: Impact parameter of a track to the vertex axis.

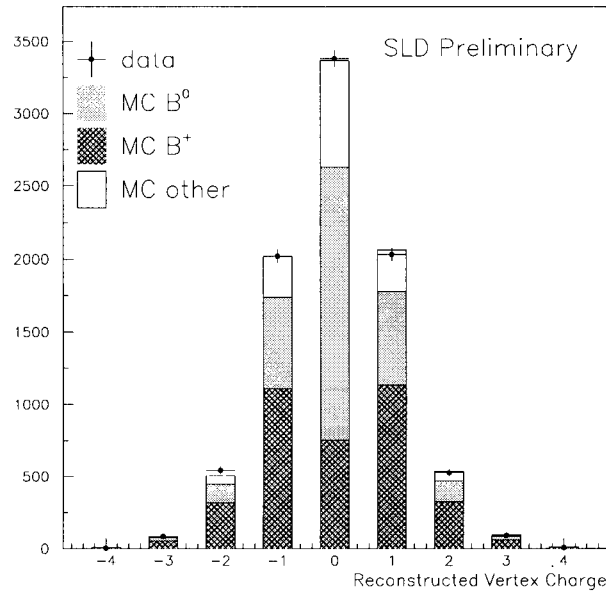


Figure 7: Distribution of charges reconstructed by the topological analysis for data (points) and Monte Carlo (histogram).

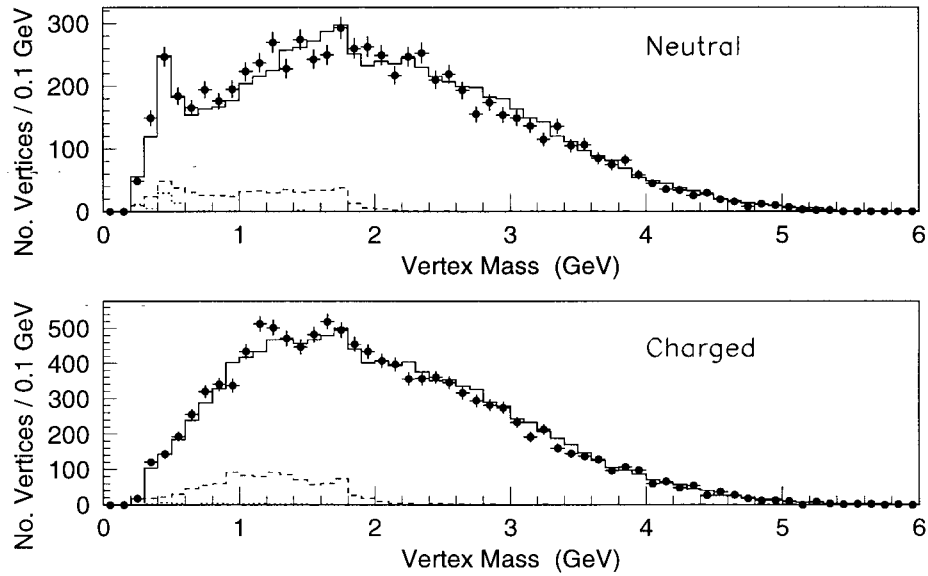


Figure 8: Mass of reconstructed secondary vertex for charged and neutral decays in the topological vertex analysis for data (points) and Monte Carlo (solid histograms). The dashed(dotted) histograms represent the charm(*uds*) contribution from Monte Carlo.

SLD Preliminary

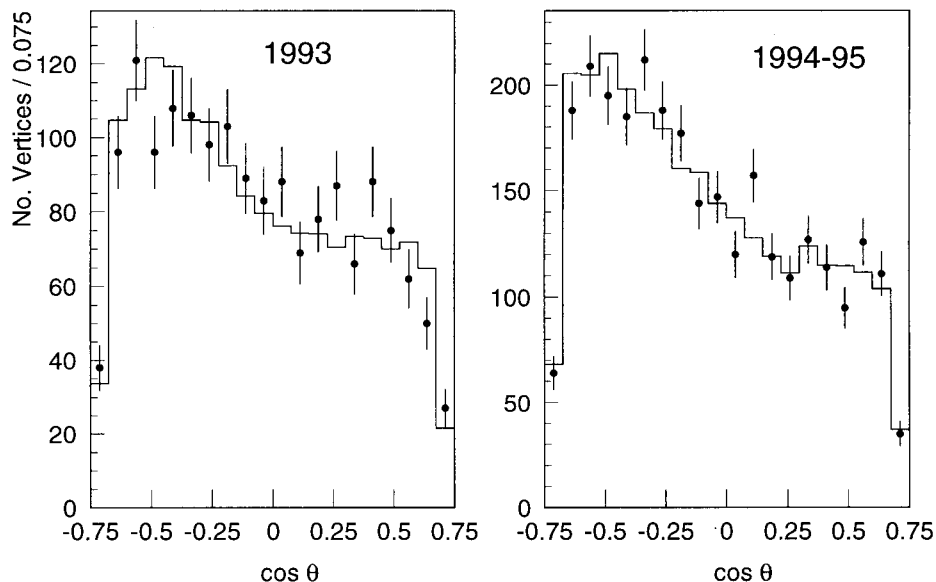


Figure 9: Distribution of  $B$  line of flight with respect to the positron beam, signed by the product of electron polarization and reconstructed charge for data (points) and Monte Carlo (histograms).

SLD Preliminary

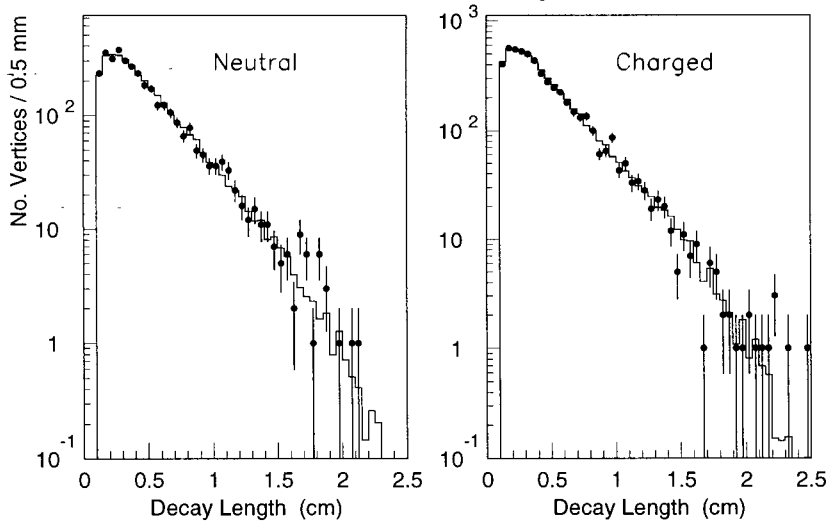


Figure 10: Decay length distributions for neutral and charged decays in the topological analysis for data (points) and Monte Carlo corresponding to the best fit (histograms).

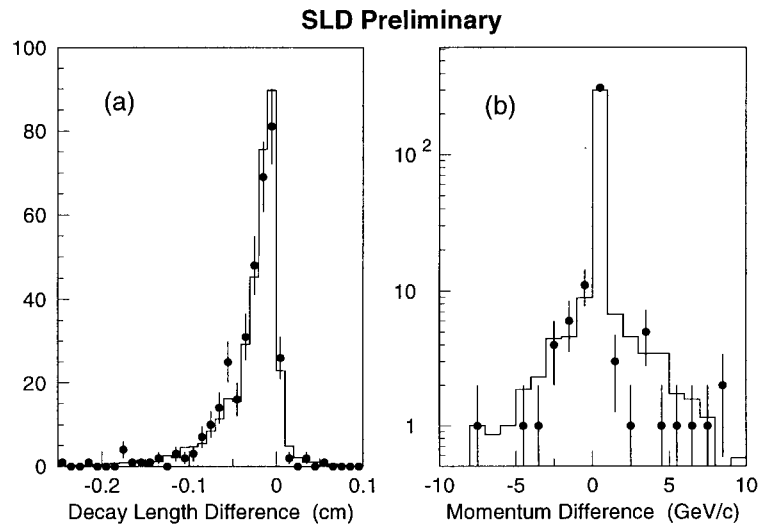


Figure 11: Distributions of the differences (semileptonic - topological) between reconstructed decay lengths and between momenta in the semileptonic and topological analyses for data (points) and Monte Carlo (histograms).

<sup>2</sup> K. Abe,<sup>(29)</sup> I. Abt,<sup>(14)</sup> C.J. Ahn,<sup>(26)</sup> T. Akagi,<sup>(27)</sup> N.J. Allen,<sup>(4)</sup> W.W. Ash,<sup>(27)†</sup>  
 D. Aston,<sup>(27)</sup> K.G. Baird,<sup>(24)</sup> C. Baltay,<sup>(33)</sup> H.R. Band,<sup>(32)</sup> M.B. Barakat,<sup>(33)</sup>  
 G. Baranko,<sup>(10)</sup> O. Bardon,<sup>(16)</sup> T. Barklow,<sup>(27)</sup> A.O. Bazarko,<sup>(11)</sup> R. Ben-David,<sup>(33)</sup>  
 A.C. Benvenuti,<sup>(2)</sup> T. Bienz,<sup>(27)</sup> G.M. Bilei,<sup>(22)</sup> D. Bisello,<sup>(21)</sup> G. Blaylock,<sup>(7)</sup>  
 J.R. Bogart,<sup>(27)</sup> T. Bolton,<sup>(11)</sup> G.R. Bower,<sup>(27)</sup> J.E. Brau,<sup>(20)</sup> M. Breidenbach,<sup>(27)</sup>  
 W.M. Bugg,<sup>(28)</sup> D. Burke,<sup>(27)</sup> T.H. Burnett,<sup>(31)</sup> P.N. Burrows,<sup>(16)</sup> W. Busza,<sup>(16)</sup>  
 A. Calcaterra,<sup>(13)</sup> D.O. Caldwell,<sup>(6)</sup> D. Calloway,<sup>(27)</sup> B. Camanzi,<sup>(12)</sup> M. Carpinelli,<sup>(23)</sup>  
 R. Cassell,<sup>(27)</sup> R. Castaldi,<sup>(23)(a)</sup> A. Castro,<sup>(21)</sup> M. Cavalli-Sforza,<sup>(7)</sup> E. Church,<sup>(31)</sup>  
 H.O. Cohn,<sup>(28)</sup> J.A. Coller,<sup>(3)</sup> V. Cook,<sup>(31)</sup> R. Cotton,<sup>(4)</sup> R.F. Cowan,<sup>(16)</sup> D.G. Coyne,<sup>(7)</sup>  
 A. D'Oliveira,<sup>(8)</sup> C.J.S. Damerell,<sup>(25)</sup> M. Daoudi,<sup>(27)</sup> R. De Sangro,<sup>(13)</sup>  
 P. De Simone,<sup>(13)</sup> R. Dell'Orso,<sup>(23)</sup> M. Dima,<sup>(9)</sup> P.Y.C. Du,<sup>(28)</sup> R. Dubois,<sup>(27)</sup>  
 B.I. Eisenstein,<sup>(14)</sup> R. Elia,<sup>(27)</sup> D. Falciai,<sup>(22)</sup> M.J. Fero,<sup>(16)</sup> R. Frey,<sup>(20)</sup> K. Furuno,<sup>(20)</sup>  
 T. Gillman,<sup>(25)</sup> G. Gladding,<sup>(14)</sup> S. Gonzalez,<sup>(16)</sup> G.D. Hallewell,<sup>(27)</sup> E.L. Hart,<sup>(28)</sup>  
 Y. Hasegawa,<sup>(29)</sup> S. Hedges,<sup>(4)</sup> S.S. Hertzbach,<sup>(17)</sup> M.D. Hildreth,<sup>(27)</sup> J. Huber,<sup>(20)</sup>  
 M.E. Huffer,<sup>(27)</sup> E.W. Hughes,<sup>(27)</sup> H. Hwang,<sup>(20)</sup> Y. Iwasaki,<sup>(29)</sup> D.J. Jackson,<sup>(25)</sup>  
 P. Jacques,<sup>(24)</sup> J. Jaros,<sup>(27)</sup> A.S. Johnson,<sup>(3)</sup> J.R. Johnson,<sup>(32)</sup> R.A. Johnson,<sup>(8)</sup>  
 T. Junk,<sup>(27)</sup> R. Kajikawa,<sup>(19)</sup> M. Kalelkar,<sup>(24)</sup> H. J. Kang,<sup>(26)</sup> I. Karliner,<sup>(14)</sup>  
 H. Kawahara,<sup>(27)</sup> H.W. Kendall,<sup>(16)</sup> Y. Kim,<sup>(26)</sup> M.E. King,<sup>(27)</sup> R. King,<sup>(27)</sup>  
 R.R. Kofler,<sup>(17)</sup> N.M. Krishna,<sup>(10)</sup> R.S. Kroeger,<sup>(18)</sup> J.F. Labs,<sup>(27)</sup> M. Langston,<sup>(20)</sup>  
 A. Lath,<sup>(16)</sup> J.A. Lauber,<sup>(10)</sup> D.W.G. Leith,<sup>(27)</sup> M.X. Liu,<sup>(33)</sup> X. Liu,<sup>(7)</sup> M. Loreti,<sup>(21)</sup>  
 A. Lu,<sup>(6)</sup> H.L. Lynch,<sup>(27)</sup> J. Ma,<sup>(31)</sup> G. Mancinelli,<sup>(22)</sup> S. Manly,<sup>(33)</sup> G. Mantovani,<sup>(22)</sup>  
 T.W. Markiewicz,<sup>(27)</sup> T. Maruyama,<sup>(27)</sup> R. Massetti,<sup>(22)</sup> H. Masuda,<sup>(27)</sup>  
 T.S. Mattison,<sup>(27)</sup> E. Mazzucato,<sup>(12)</sup> A.K. McKemey,<sup>(4)</sup> B.T. Meadows,<sup>(8)</sup>  
 R. Messner,<sup>(27)</sup> P.M. Mockett,<sup>(31)</sup> K.C. Moffeit,<sup>(27)</sup> B. Mours,<sup>(27)</sup> G. Müller,<sup>(27)</sup>  
 D. Muller,<sup>(27)</sup> T. Nagamine,<sup>(27)</sup> U. Nauenberg,<sup>(10)</sup> H. Neal,<sup>(27)</sup> M. Nussbaum,<sup>(8)</sup>  
 Y. Ohnishi,<sup>(19)</sup> L.S. Osborne,<sup>(16)</sup> R.S. Panvini,<sup>(30)</sup> H. Park,<sup>(20)</sup> T.J. Pavel,<sup>(27)</sup>  
 I. Peruzzi,<sup>(13)(b)</sup> M. Piccolo,<sup>(13)</sup> L. Piemontese,<sup>(12)</sup> E. Pieroni,<sup>(23)</sup> K.T. Pitts,<sup>(20)</sup>  
 R.J. Plano,<sup>(24)</sup> R. Prepost,<sup>(32)</sup> C.Y. Prescott,<sup>(27)</sup> G.D. Punkar,<sup>(27)</sup> J. Quigley,<sup>(16)</sup>  
 B.N. Ratcliff,<sup>(27)</sup> T.W. Reeves,<sup>(30)</sup> J. Reidy,<sup>(18)</sup> P.E. Rensing,<sup>(27)</sup> L.S. Rochester,<sup>(27)</sup>  
 J.E. Rothberg,<sup>(31)</sup> P.C. Rowson,<sup>(11)</sup> J.J. Russell,<sup>(27)</sup> O.H. Saxton,<sup>(27)</sup> S.F. Schaffner,<sup>(27)</sup>  
 T. Schalk,<sup>(7)</sup> R.H. Schindler,<sup>(27)</sup> U. Schneekloth,<sup>(16)</sup> B.A. Schumm,<sup>(15)</sup> A. Seiden,<sup>(7)</sup>  
 S. Sen,<sup>(33)</sup> V.V. Serbo,<sup>(32)</sup> M.H. Shaevitz,<sup>(11)</sup> J.T. Shank,<sup>(3)</sup> G. Shapiro,<sup>(15)</sup>  
 S.L. Shapiro,<sup>(27)</sup> D.J. Sherden,<sup>(27)</sup> K.D. Shmakov,<sup>(28)</sup> C. Simopoulos,<sup>(27)</sup> N.B. Sinev,<sup>(20)</sup>  
 S.R. Smith,<sup>(27)</sup> J.A. Snyder,<sup>(33)</sup> P. Stamer,<sup>(24)</sup> H. Steiner,<sup>(15)</sup> R. Steiner,<sup>(1)</sup>  
 M.G. Strauss,<sup>(17)</sup> D. Su,<sup>(27)</sup> F. Suekane,<sup>(29)</sup> A. Sugiyama,<sup>(19)</sup> S. Suzuki,<sup>(19)</sup>  
 M. Swartz,<sup>(27)</sup> A. Szumilo,<sup>(31)</sup> T. Takahashi,<sup>(27)</sup> F.E. Taylor,<sup>(16)</sup> E. Torrence,<sup>(16)</sup>  
 J.D. Turk,<sup>(33)</sup> T. Usher,<sup>(27)</sup> J. Va'vra,<sup>(27)</sup> C. Vannini,<sup>(23)</sup> E. Vella,<sup>(27)</sup> J.P. Venuti,<sup>(30)</sup>  
 R. Verdier,<sup>(16)</sup> P.G. Verdini,<sup>(23)</sup> S.R. Wagner,<sup>(27)</sup> A.P. Waite,<sup>(27)</sup> S.J. Watts,<sup>(4)</sup>  
 A.W. Weidemann,<sup>(28)</sup> E.R. Weiss,<sup>(31)</sup> J.S. Whitaker,<sup>(3)</sup> S.L. White,<sup>(28)</sup> F.J. Wickens,<sup>(25)</sup>  
 D.A. Williams,<sup>(7)</sup> D.C. Williams,<sup>(16)</sup> S.H. Williams,<sup>(27)</sup> S. Willocq,<sup>(33)</sup> R.J. Wilson,<sup>(9)</sup>  
 W.J. Wisniewski,<sup>(5)</sup> M. Woods,<sup>(27)</sup> G.B. Word,<sup>(24)</sup> J. Wyss,<sup>(21)</sup> R.K. Yamamoto,<sup>(16)</sup>  
 J.M. Yamartino,<sup>(16)</sup> X. Yang,<sup>(20)</sup> S.J. Yellin,<sup>(6)</sup> C.C. Young,<sup>(27)</sup> H. Yuta,<sup>(29)</sup>  
 G. Zapalac,<sup>(32)</sup> R.W. Zdarko,<sup>(27)</sup> C. Zeitlin,<sup>(20)</sup> Z. Zhang,<sup>(16)</sup> and J. Zhou,<sup>(20)</sup>

- (1) *Adelphi University, Garden City, New York 11530*  
 (2) *INFN Sezione di Bologna, I-40126 Bologna, Italy*  
 (3) *Boston University, Boston, Massachusetts 02215*  
 (4) *Brunel University, Uxbridge, Middlesex UB8 3PH, United Kingdom*  
 (5) *California Institute of Technology, Pasadena, California 91125*  
 (6) *University of California at Santa Barbara, Santa Barbara, California 93106*  
 (7) *University of California at Santa Cruz, Santa Cruz, California 95064*  
 (8) *University of Cincinnati, Cincinnati, Ohio 45221*  
 (9) *Colorado State University, Fort Collins, Colorado 80523*  
 (10) *University of Colorado, Boulder, Colorado 80309*  
 (11) *Columbia University, New York, New York 10027*  
 (12) *INFN Sezione di Ferrara and Università di Ferrara, I-44100 Ferrara, Italy*  
 (13) *INFN Lab. Nazionali di Frascati, I-00044 Frascati, Italy*  
 (14) *University of Illinois, Urbana, Illinois 61801*  
 (15) *Lawrence Berkeley Laboratory, University of California, Berkeley, California 94720*  
 (16) *Massachusetts Institute of Technology, Cambridge, Massachusetts 02139*  
 (17) *University of Massachusetts, Amherst, Massachusetts 01003*  
 (18) *University of Mississippi, University, Mississippi 38677*  
 (19) *Nagoya University, Chikusa-ku, Nagoya 464 Japan*  
 (20) *University of Oregon, Eugene, Oregon 97403*  
 (21) *INFN Sezione di Padova and Università di Padova, I-35100 Padova, Italy*  
 (22) *INFN Sezione di Perugia and Università di Perugia, I-06100 Perugia, Italy*  
 (23) *INFN Sezione di Pisa and Università di Pisa, I-56100 Pisa, Italy*  
 (24) *Rutgers University, Piscataway, New Jersey 08855*  
 (25) *Rutherford Appleton Laboratory, Chilton, Didcot, Oxon OX11 0QX United Kingdom*  
 (26) *Sogang University, Seoul, Korea*  
 (27) *Stanford Linear Accelerator Center, Stanford University, Stanford, California 94309*  
 (28) *University of Tennessee, Knoxville, Tennessee 37996*  
 (29) *Tohoku University, Sendai 980 Japan*  
 (30) *Vanderbilt University, Nashville, Tennessee 37235*  
 (31) *University of Washington, Seattle, Washington 98195*  
 (32) *University of Wisconsin, Madison, Wisconsin 53706*  
 (33) *Yale University, New Haven, Connecticut 06511*
- † Deceased
- (a) *Also at the Università di Genova*  
 (b) *Also at the Università di Perugia*